



Effect of etching parameters on the electrochemical response of silicon nanowires

Fatma Zaïbi^{1,2,3,5} · Ichrak Slama^{2,4} · Natalia Beshchasna⁵ · Jörg Opitz⁵ · Martin Mkandawire³ · Radhouane Chtourou²

Received: 3 March 2021 / Accepted: 25 September 2021 / Published online: 3 November 2021
© The Author(s), under exclusive licence to Springer Nature B.V. 2021

Abstract

Silicon nanowires combine a high electrical conductivity with low thermal conductivity due to the small cross section offering a good template for sensing. Silicon p-type (100) substrate was used in this work to present a comparative study from a morphological point of view as well as for the electrical properties of silicon nanowires (SiNWs) etched by Ag-assisted chemical method in one-step and two-step process. The comparison between both techniques for SiNWs samples' elaborated with Metal-Assisted Chemical Technique (MACE) was investigated by Scanning Electron Microscopy images that clearly show the presence of nanowires and the existence of porous silicon structure especially by Transmission Electron Microscopy technique. Several particles on the SiNWs surface such as oxygen and hydrogen elements were identified by Fourier-Transformed Infrared Spectroscopy measurements. The results indicate that the MACE's steps influence the nucleation and motility of Ag particles, which leads to a different length and density structure within the nanowires. These parameters influence the electrochemical properties of the surface that was studied using electrochemical measurements. Impedance analysis revealed that the charge transfer resistance decreases with the length of the SiNWs dissimilar to the capacitance based on the cyclic voltammetry analysis. In this paper, we studied the electrochemical parameters which indicate that two-step MACE procedure presents a resistance nearly the half of the value of SiNWs produced using one-step MACE technique; as for the capacitance, it increases by 28.5%. We can notice that SiNWs produced using two-step MACE show better results for biosensing application. For that reason, we decide to functionalize the two-step MACE SiNWs to prove the ease of the surface modification. Deposition of nickel nanoparticles was analysed manifesting a good amelioration of the resistance with a factor of 2.5.

✉ Fatma Zaïbi
zaibifatma6@gmail.com

Ichrak Slama
ichrakslama@live.com

Natalia Beshchasna
natalia.beshchasna@ikts.fraunhofer.de

Jörg Opitz
joerg.opitz@ikts.fraunhofer.de

Martin Mkandawire
martin_mkandawire@cbru.ca

Radhouane Chtourou
radhouane.chtourou@crten.nrnt.tn

¹ Tunis University - National High School of Engineering of Tunis, 5 Av Taha Hussein, 1008 Tunis, Tunisia

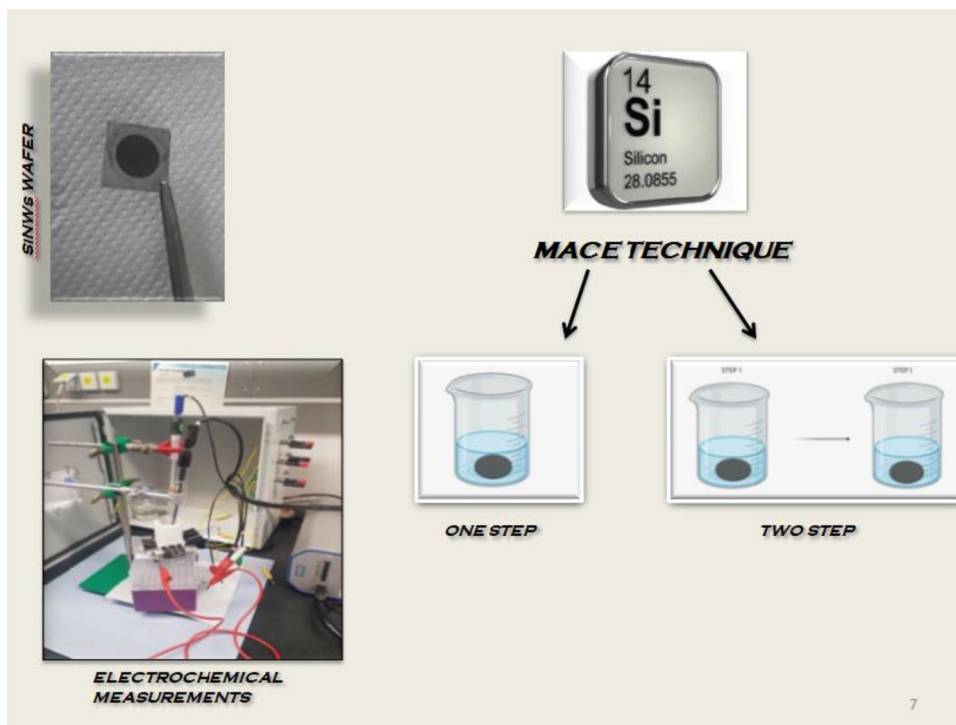
² Nanomaterials and Systems for Renewable Energy Laboratory, The Research and Technology Centre of Energy, Technopole De Borj-Cédria, BP 95, Hammam Lif, Borj-Cedria, 2050 Tunis, Tunisia

³ Department of Chemistry, School of Science and Technology, Cape Breton University, Sydney, NS B1P 6L2, Canada

⁴ Laboratory of Transmissible Diseases and Biologically Active Substances, Faculty of Pharmacy, University of Monastir, LR99ES27, 5000 Monastir, Tunisia

⁵ Fraunhofer Institute for Ceramic Technologies and Systems IKTS, Maria-Reiche Street 2, 01109 Dresden, Germany

Graphic abstract



Keywords Silicon nanowires · One-step MACE · Two-step MACE · EIS

1 Introduction

Several research [1, 2] works have focused lately on developing and understanding the manipulation of one-dimensional structures such as silicon nanowires (SiNWs), and it represents the most used semiconductor in the nanotechnology. Specially, vertically aligned SiNWs that possess unique physical and chemical properties. Consequently, vertically aligned SiNWs arrays have a variety of potential applications, such as in electronics [3, 4], chemical and biological sensing with high sensitivity [5–7], photovoltaic devices [8], thermoelectric applications [9, 10], and rechargeable lithium-ion battery [11, 12].

The vertically aligned SiNWs can be fabricated by top-down etching of planar wafers, using methods like reactive ion etching [13] and electron beam lithography [14], or from the bottom-up approaches using methods like vapour–liquid–solid growth [15], which induce epitaxial growth on lattice-matched substrates. Although synthesis of nanowires by vapour–liquid–solid process permits the modulation of dopants along the nanowire growth axis. The synthesis of vertically aligned SiNWs with complex morphology is quite challenging, requiring control over multiple interdependent aspects of the process. Thus, these techniques, including

vapour–liquid–solid, generally present some limitations that require high synthesis temperatures or high vacuum templates, complex equipment, and long synthesis time. Consequently, the synthesis of vertically aligned SiNWs using metal-assisted chemical etching (MACE) method has gained considerable prominence in the past decades, due to its simplicity and low cost, and offering excellent controllability of SiNWs structure and morphology (e.g. length, diameter, cross-sectional shape, orientation, porosity and crystalline quality) [16–18]. Besides, MACE does not introduce any obvious crystallographic defects induced by the etching solution or any limitation to the nanowire’s size. Furthermore, the fabrications using the MACE method has led to emergency mesoporous SiNWs, which widened applications SiNWs derived from the enhanced surface areas and quantum confinement effect.

In general, the MACE method [19] involves two successive steps, the nucleation of metal catalysts and anisotropic etching, which can be either one-step (direct etching) [20] or two-step (deposition and etching) MACE [21], here-in-after abbreviated 1-MACE and 2-MACE, respectively. The difference between these two methods lies mainly in the number of process steps, with the 2-MACE method having more. The 1-MACE has two processes that take place in

an etching solution containing HF and metal salts. In contrast, the 2-MACE has metal catalysts firstly deposited on the wafer surface, and the subsequent anisotropic etching occurs in the HF/oxidant solution, where the oxidant can be either H_2O_2 , $\text{Fe}(\text{NO}_3)_3$ or KMnO_4 [22, 23]. The 2-MACE is the most used method.

A few studies have confirmed that the morphology of SiNWs generally depends on the doped type (i.e. doped p-type or n-type silicon) and concentration, fabrication methods, and etching temperature [24]. In general, the roughness of SiNWs increases with increasing doped level and H_2O_2 concentration [25, 26]. However, little has been reported in the literature on how fabrication method and etching temperature affect the silicon nanowire's morphology. Bearing in mind that the morphology and structure are fundamental to the optical [27], electrical [28], and thermal properties [29] of semiconductor nanowires, it is worth to ascertain if using 1-MACE and 2-MACE has ramification on the morphological and corresponding electrochemical properties of synthesized SiNWs. Hence, we communicate in this work a comparative study of the influence of the 1-MACE and 2-MACE techniques of SiNWs elaboration on the morphology as well as the electrochemical properties.

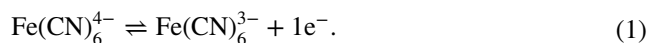
2 Materials and methods

P-type silicon wafers, with (100) orientations and resistivity of 1–20 Ωcm , were selected for this study. An aluminium layer was deposited on the backside of the substrate using a VINCI thermal evaporator (VINCI Technologies, France). Prior to etching, silicon was cleaned with ultrasonication using acetone, ethanol, and deionized water, respectively. For the one-step MACE technique, the clean wafers were attached to a Teflon cell and immersed in the etchant solution containing 40% HF, 0.035 mol/L of AgNO_3 and 10 mol/L of H_2O_2 , under ambient temperature. As for the two-step technique, the clean substrates were immersed in a 40% HF, 0.035 mol/L solution for several minutes for silver layer deposition on the silicon wafer, then, dipped it in a 40% HF, and 10 mol/L H_2O_2 solution. The samples were subsequently immersed into 35% HNO_3 to dissolve the as-generated Ag dendrites. Finally, the wafers were thoroughly rinsed with deionized water and dried under N_2 stream.

The morphology of the nanostructure's silicon template (1 cm^2) as well as the synthesized SiNWs was subsequently investigated using SEM (JEOL 5900LV SEM, Tokyo, Japan), X-ray diffraction XRD (Bruker D8 advance X-Ray Diffractometer, Billerica, MA, USA) with $\text{CuK}\alpha$ ($\lambda = 1.54\text{ \AA}$) in 2θ ranging from 40 to 80° for the SiNWs structure. The surface functional groups and modification were investigated using FTIR (Bruker IFS66v/s FTIR spectrometer, Billerica, MA, USA). The FTIR analysis was

conducted in reflectance mode from 400 to 4000 cm^{-1} at 4 cm^{-1} interval. The electrochemical analysis was performed using a Galvanostat potentiostat Solartron Analytical.

An electrochemical cell with three electrodes system was used. The SiNWs, Pt wire, and Ag/AgCl (5 M KCl) electrodes were identified as the working electrode, the counter electrode, and the reference electrode, respectively. All electrodes were thoroughly cleaned before use. Measurements were carried out in ionic solution 2.5 mM potassium ferricyanide/ferricyanide redox couple in 1 M PBS described by the following formula:



3 Results and discussions

The SEM image (Fig. 1) presents the one-dimensional silicon nanowires made by both one-step and two-step MACE method. For both processes, SiNWs are in an orderly and vertical orientation replying to the (100) orientation of the silicon wafer as confirmed by the XRD pattern (Fig. 1c) revealing only one diffraction peak at $2\theta = 69^\circ$ which corresponds to the (400) silicon plane orientation. These results demonstrate that the MACE technique produces a single crystal core that replicates the crystallographic orientation of the substrate. Besides, the density of the nanowires shows the better distribution for two-step technique as proven on SEM images (Fig. 1a), as well as for the uniformity in terms of the nanowire diameter and length. Figure 1a clearly demonstrates such highly uniform and vertically aligned Si nanowires made with the two-step method (with diameters in the range of 450 nm and lengths of 36 μm) on a large scale. Concerning one-step Si nanowires, Fig. 1b shows a lack from the point of view of uniformity and density due to excessive dissolution of Si by the etchant solution. In one-step as well as in two-step MACE procedure, the nanowires are vertically aligned with diameters in the range 100 nm and lengths about 18 μm .

The roots of SiNWs fabricated by one-step and two-step MACE technique (Fig. 2a) represent a solid and smooth surface as well as a porous structure along the wire produced by the nucleation of Ag^+ ion and the Si dissolution. This aspect is given by the use of H_2O_2 which plays an essential role in the fabrication of SiNWs as well as its morphology (Fig. 2a and b). The presence of H_2O_2 in etchant can generate numerous Ag^+ ions according to the following reaction:

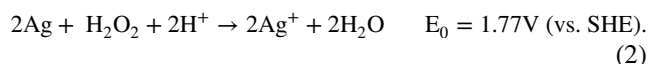
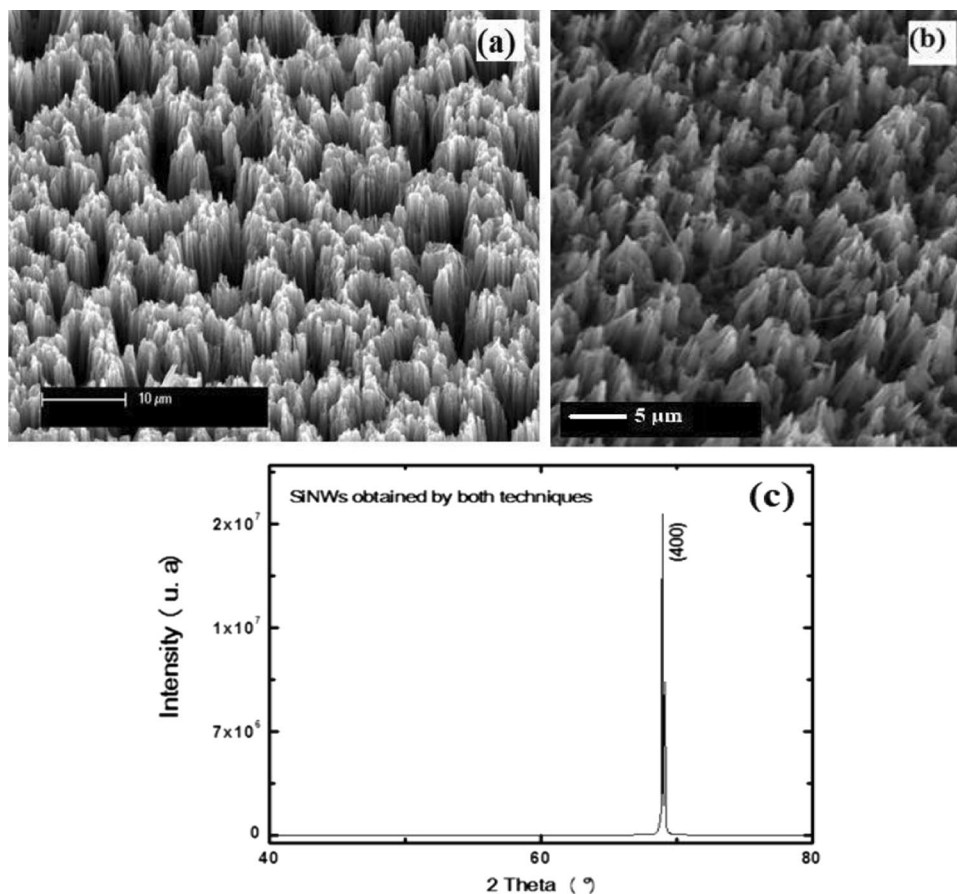


Fig. 1 The SiNWs fabricated using **a** two-step MACE, **b** one-step MACE method; and **c** the XRD pattern confirming the SiNWs synthesized by both MACE techniques



Some of the Ag^+ ions produced spread through the nanowires and nucleate on its surface under the catalysis of Ag nanoparticles, which leads to the structure of pores formed around the nanowire. By the use of Fourier Transform Infrared spectroscopy (FTIR) (Fig. 2c and d), it is possible to prove the existence of the same bonds for both techniques. It shows a Si–Si bond at 653 cm^{-1} , a remarkable bond at 1073 cm^{-1} , 1167 cm^{-1} and 3389 cm^{-1} corresponding to Si–Ox, Si–O–Si, and O–H, respectively. C–H and C–H_x bonds at 1369 cm^{-1} , 1633 cm^{-1} , and 2277 cm^{-1} are present due to environmental contamination and can hardly be avoided. The N–H bond at 1462 cm^{-1} confirmed that a few N atoms are linked to Si after the reaction of SiNWs with HNO_3 . Nevertheless, we can notice a difference in the intensity; in one step, the bonds were well distinguished and intense than those in the two-step process. This

phenomenon can be explained by the high density of SiNWs, as shown in the SEM image (Fig. 1), which increases the possibilities of internal light interactions at the surface of the SiNWs and leading to a decrease in absorption within this nanostructures.

The formation of SiNWs by MACE technique is explained by the different exchange of ions between the etchant and the Si surface. From that point, we can explain the difference of the lengths of SiNWs made by one-step MACE technique, about $18\text{ }\mu\text{m}$ as lengths with 100 nm as their diameters, and $36\text{ }\mu\text{m}$ with 450 nm , respectively, for the two-step method.

The silver layer deposition resumes the two-step MACE technique and then the caving of silver nanoparticles and production of SiNWs.

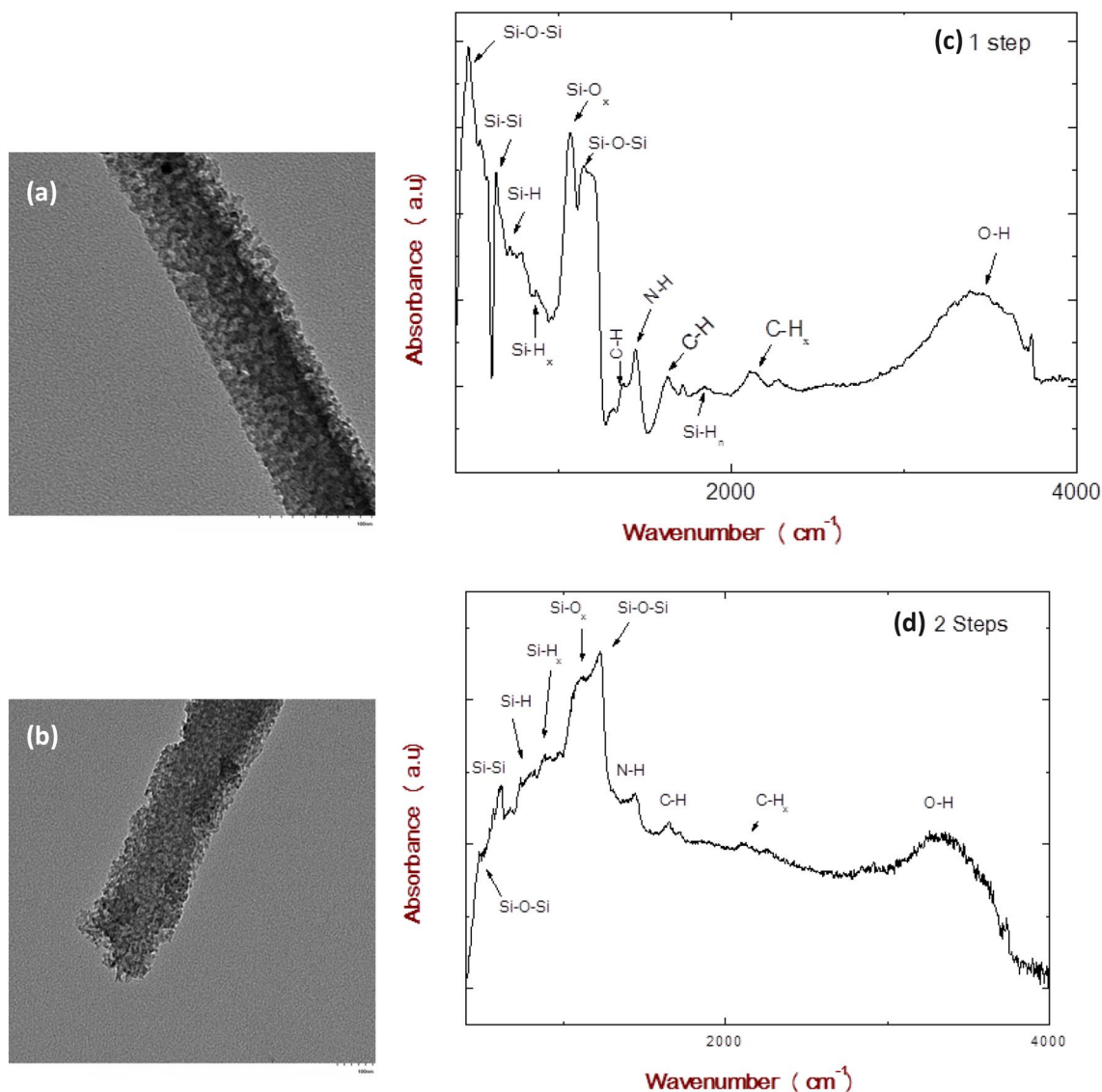
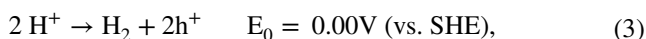
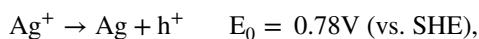


Fig. 2 FTIR spectra revealing the surface functional groups for **a** SiNWs etched in one-step MACE, **b** SiNWs etched in two-step MACE. **c**, **d** TEM images showing the presence of the pores along the nanowire for one step and two-step MACE technique

At the AgNO_3/HF electrolyte solution interface, the production of H_2 particles is accompanied by the injection of holes in the valence band of silicon and leads to its oxidation and then it dissolves into silicon hexafluoride ions (SiF_6^{2-}) in an aqueous solution of hydrofluoric acid. Throughout the dissolving process, Ag particles flow underneath to bulk silicon, defining irregularly porous grooves covered with Ag microstructures. Thus, these Ag nanoparticles play the role of cathode and the silicon then plays the role of the anode. The following two reactions can formulate the electrochemical redox reaction:

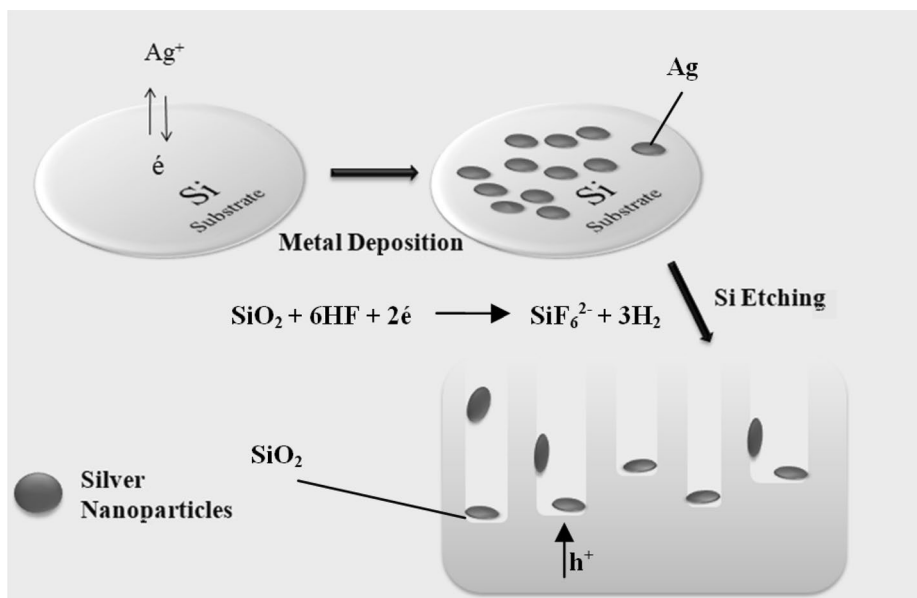
a. silver/electrolyte interface, the cathode reactions are described by



b. silicon/silver interface, the anode reaction is given by



Overall reaction

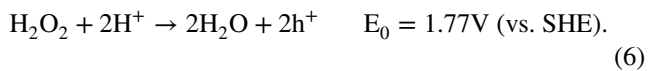


Once all Ag^+ ions confront Ag particles or silicon surface and have reduced to Ag, the oxidation of silicon becomes very slow, leading to a decrease in the etching speed of the silicon. Hence, the need of an additional hole injection to allow the continuation of silicon nanostructuring.

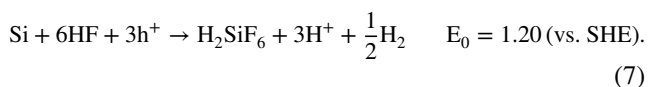
In consideration of the important role of H_2O_2 in the fabrication of SiNWs, which affects not only the etching rate, but also the morphology, nanostructure, and orientation of SiNWs, the addition of hydrogen peroxide is then the second step related to the two-step MACE technique.

Si atoms underneath Ag nanoparticles hold holes produced from the reduction of hydrogen peroxide (H_2O_2). We can explain the dissolution process by the more positive redox potential of H_2O_2 (1.77 V vs standard hydrogen electrode (SHE)) than that of Ag^+ (0.78 V vs SHE) which leads to the injection of more holes into the Si valence band through the Ag particle surface. The process is described by the following reactions:

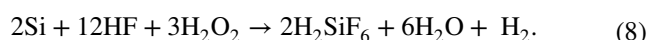
At the silver/electrolyte interface, the cathode reaction:



At the silicon/silver interface, the anode reaction:



The overall reaction can be represented by



As for the $\text{HF}/\text{AgNO}_3/\text{H}_2\text{O}_2$ solution (one-step MACE technique), both Ag^+/Ag and $\text{H}_2\text{O}_2/\text{H}_2\text{O}$ couples have higher positive equilibrium potentials than silicon EVB (Equilibrium Valence Band). Thus, the holes will be injected into the valence band of silicon followed with the deposition of Ag particles and the reduction of H_2O_2 , which induces silicon substrate oxidation and dissolution and then the simultaneous growth of the SiNWs and the formation of porosity.

The generated Ag nanoparticles on the surface of silicon play the role of microcathodes and catalyse H_2O_2 reduction at the surface. The uptake of the proton (H^+) and the electrons in the process are described by reaction (6) explained by the difference of the potential between the cathode site, $E(\text{H}_2\text{O}_2) = 1.77\text{ V vs SHE}$, which is higher than that of the anode site, $E(\text{Si}) = 1.2\text{ V vs SHE}$. Therefore, a local corrosion current is exchanged between the cathode and the anode sites explaining the role of Ag particle as a redox centre and its behaviour as a short-circuited galvanic cell with an electron flow inside the Ag particle. Likewise, H^+ protons would migrate out of the Ag particle from the anode site to the cathode site providing a gradient across the Ag particle between anodic and cathodic sites. This gradient is considered to be the source of an electric field that propels the Ag particles (with a negative charge) to the anode site. Thus, the migration of Ag particles and its deposition on the surface and the sides of SiNWs is assured in a vertical or horizontal direction, respectively. Thus, the formation process

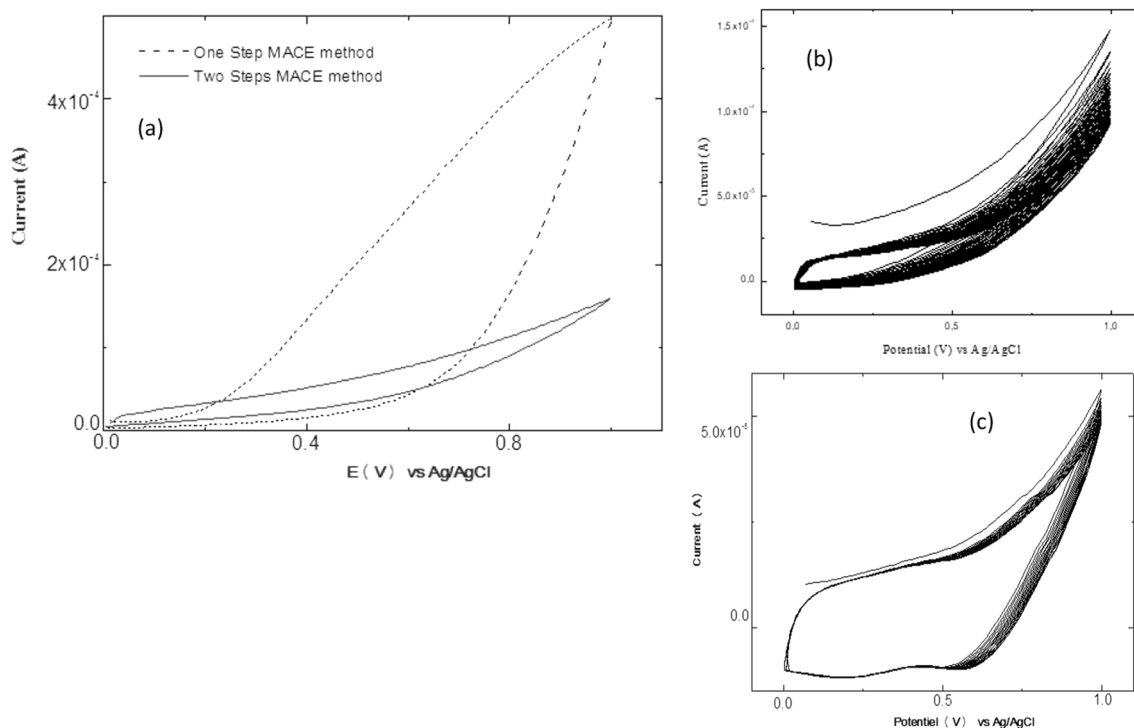


Fig. 3 Cyclic voltammety scan of **a** one-step and two-step MACE etching, **b** stability of one-step MACE technique and **c** stability of two-step MACE technique in 2.5 mM ferri-ferrocyanide, 0.1 M PBS electrolyte

of mesoporous structures within the SiNWs was consistent with that of microporous structures. Both are caused by the lateral etching of silicon, i.e. lateral mobility of Ag particles.

3.1 Electrochemical studies

Electrochemical spectroscopy was performed to study the differential capacity as a function of potential in the SiNWs and the charge transfer resistance at the surface.

The cyclic voltammety presented in Fig. 3, of the two samples fabricated by the two processes, showed a continuous curve without any redox peak which is attributed to the electric double-layer formation at the electrode/electrolyte interfaces. We can notice in the figure that the SiNWs, produced by the one-step MACE technique, produce a higher current than the two-step MACE technique explained by the difference in density between the two surfaces as proved by the SEM technique. The following equation calculates the specific capacitance, C [30]:

$$C = \frac{(I_+ + I_-)}{vA} \quad (9)$$

C is the capacitance per unit area, v is the scan rate, I_+ and I_- are the average current measured during charging

and discharging states, and A is the electrode area. Figure 3b and c indicates the excellent stability of SiNWs for both techniques.

To better understand the capacitance mechanism and the electrochemical properties of these chemically growing SiNWs, EIS can be used when a semiconductor / liquid interface is presented by studying the system's response under a perturbation of alternating current (AC) of different frequencies which can identify various electronic states in the semiconductor in a quantitative or quasi-quantitative manner.

The EIS results are shown in Fig. 4. It was conducted, at room temperature, over a frequency range of 1 Hz to 100 kHz with 5 mV signal amplitude. This choice of amplitude was contributed to minimize the perturbations of signals. The impedance features can be discussed in terms of Nyquist plots.

As described in the SEM images (Fig. 1), the SiNWs electrode morphology is comparable to a thin film presenting a mixture of ionic/electronic conductor with a large surface area and pores that can be partially filled by the liquid electrolyte. The impedance analysis shows the contribution of both surface resistance and diffusion through the nanowires, which is usually limiting the kinetics of the ions exchange between the surface (SiNWs) and the electrolyte. Therefore, in our case, the equivalent electric circuit is given

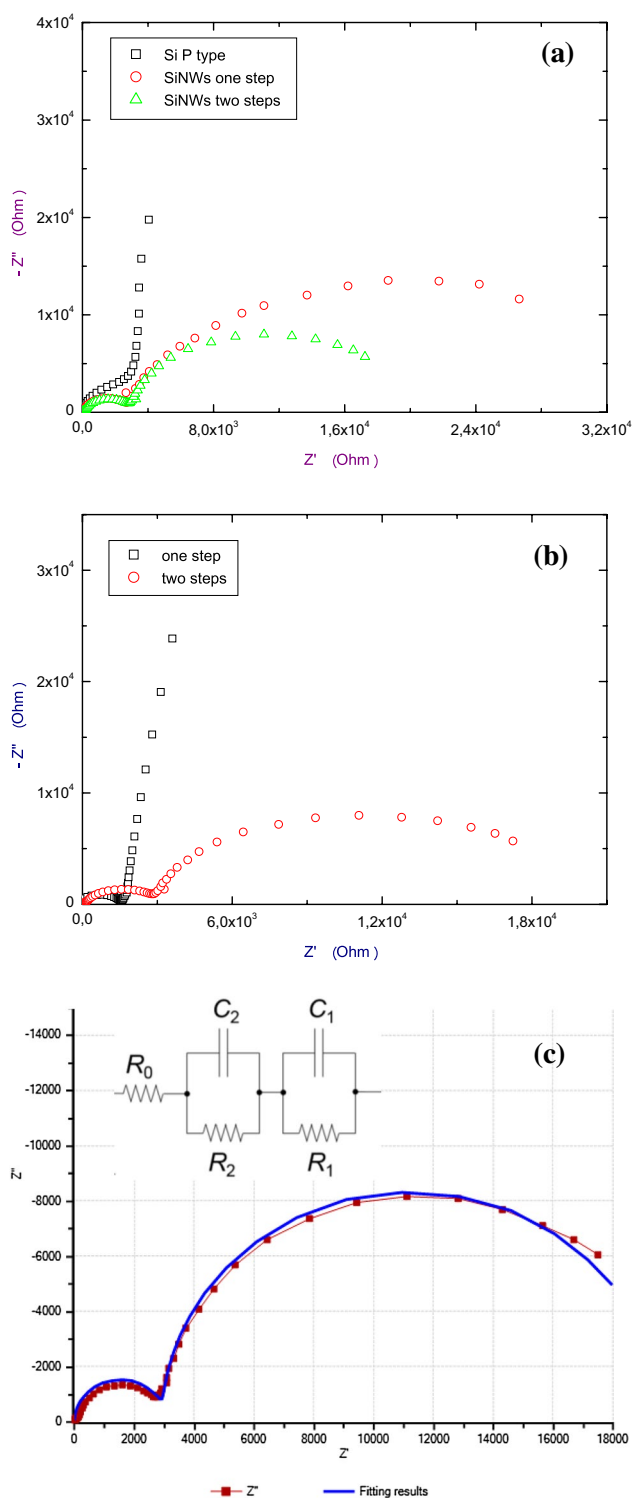


Fig. 4 a, b EIS Nyquist plots of one-step and two-step MACE technique for SiNWs and c Fitting curve of EIS result of silicon nanowires

in Fig. 4c describing the two semicircles of the Nyquist plot of SiNWs, where C₁ is the double-layer capacitance of the NWs/electrolyte interface, R₁ is the resistance of the NWs

Table 1 The parameters of the equivalent circuit of Nyquist plots of bare Si type P, SiNWs one-step etching, and SiNWs two-step etching

	R ₁ (Ohm)	R ₂ (Ohm)	C ₁ (μF)	C ₂ (μF)
Bare Si type P	1.91 × 10 ⁵	2.82 × 10 ³	0.056	0.019
SiNWs one-step etching	2.77 × 10 ⁴	3.44 × 10 ³	2.473	0.060
SiNWs two-step etching	1.62 × 10 ⁴	3.00 × 10 ³	3.176	0.065

surface (charge transfer between the electrolyte and NWs), and C₂ and R₂ represent the impedance element reporting the diffusion process inside the NWs.

At high frequencies, the diameter of the semicircle is tiny reflecting low charge transfer. Thus, the working electrode acts like a resistor and the impedance is dominated by the resistance of the system, which changes negligibly with the increase of frequency (Fig. 4b). It can be explained by the electronic conduction between the substrate (Si), the active material (SiNWs), and the ionic conduction through the electrolyte. This resistive behaviour of the surface is presented by a resistance in parallel with the double-layer capacitance in the equivalent circuit. It appears in the Nyquist graph as a semicircle with a diameter equal to the value of the surface resistance.

At lower frequencies (below 10 Hz), the surface shows a capacitive behaviour due to the contribution of diffusion, which is present due to the migration of electrolyte ions into the bulk of SiNWs active material. The determination of the surface parameters can be made by fitting procedures using the equivalent circuit in Fig. 4d. The former approach has the advantage that the errors in the parameter have electrical units allowing us to evaluate their significance.

In our model, the determination of the surface parameters has a numerical mistake that is usually lower than 1%. By analysing Table 1, we can notice that, for the first semicircle, the SiNWs fabricated by two-step MACE technique present a resistance nearly the half of the resistance value of SiNWs produced using one-step MACE technique. As for the capacitance of the SiNWs fabricated by two-step MACE technique, it increases by 28.5%. The rise of the capacitance is defined by the increase of the surface area of NWs, which is proportionally varied to the density and length of NWs ($n \times 2R \times L$, where n represents the number of NWs in a plan-view SEM image, R the radius of NWs, and L the length of NWs). The equation permits us to calculate the increased surface area that interacts with the solution. However, for the NWs that present longer length generate a poor CV measurement due to the creation of the leakage current reached by long NWs which failed caused by mechanical stress and vibration. Hence, the difference in the electrochemical properties of the NWs fabricated by one-step and two-step MACE technique allows concluding the better suitability of the second method for biosensing application due to the

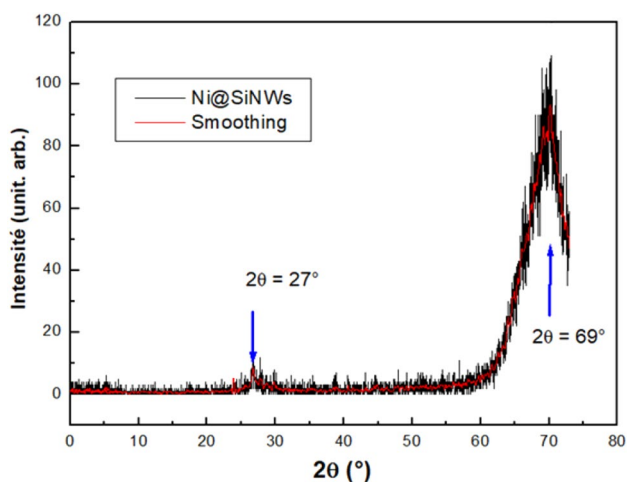


Fig. 5 The XRD pattern confirming the adsorption of Ni on SiNWs synthesized by two-step technique

important charge transfer amelioration of the surface. As for NWs fabricated by one-step MACE technique, it shows better result for the CV characterizations, which leads it to offer a good template for pH sensing.

In addition to the enhancement of the electrochemical parameters of Si surface, the open-circuit voltage (OCV) also changed with the surface modification. From -0.079 V for Si to -0.350 V and 0.182 V for SiNWs fabricated by one-step and two-step MACE, respectively. The open-circuit voltage increases as the band gap increases. Therefore, a comparison of open-circuit potential confirmed the fast kinetics of two-step SiNWs/electrolyte interface and, thus, a suitable template for biosensing application.

Those attractive achievements suggest the exciting potential of SiNWs as a promising platform for various

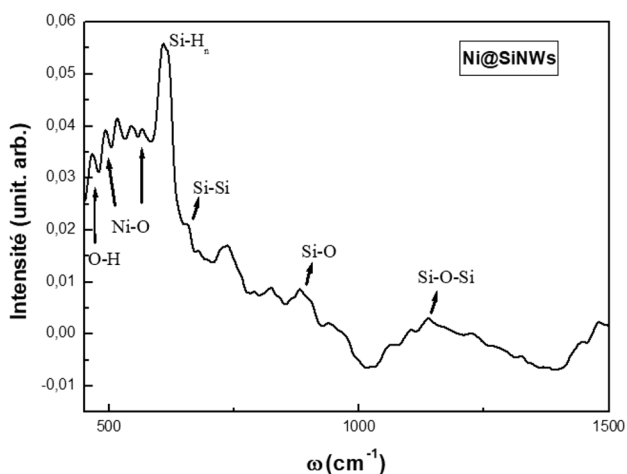
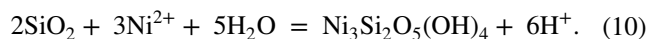
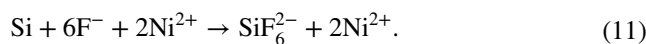


Fig. 6 FTIR spectra revealing the surface functional groups for Ni@SiNWs

applications [29]. In this part of this work, we present a novel kind of electrochemical nano-sensor using Ni@SiNWs as a high-quality nano-electrode assemble [31]. The SiNWs two step was selected for this part due to the critical resistivity amelioration that represents compared to the one-step electrical properties. This template was immersed in an ionic solution of nickel. The XRD spectra of Ni@SiNWs (Fig. 5) show a new diffraction peak at 27° which can only be attributed to the NiSi_2 bond showing the reaction between SiNWs and the Ni^{2+} cations during adsorption:



FTIR spectroscopy was used to study the interaction between different species and changes in the chemical composition of the surface. In our study, it was to prove the presence of Ni particles after adsorption. Figure 6 shows the IR spectrum of the Ni @ SiNWs surface in the interval $[400, 1500] \text{ cm}^{-1}$. A new absorption bands at 492 cm^{-1} and 568 cm^{-1} are generally attributed to Ni–O bonds. A band located at 462 cm^{-1} corresponds to the O–H bond which can only be due to the $\text{Ni}(\text{OH})_2$ bond. The bands at 609 cm^{-1} , 824 cm^{-1} , 885 cm^{-1} , and 1140 cm^{-1} correspond to the Si–H_n, Si–O, Si–O, and Si–O–Si bonds, respectively. Therefore, the FTIR results confirm the adsorption of Ni particles on the SiNWs surface. EIS measurements were performed to determine the internal resistance of the electrode as reported in Fig. 7a. It proves the adsorption of NiNPs on the SiNWs surface via the reaction as expressed in reaction 10:



The fitting curve followed by the Randles equivalent circuit shows two distinct (Fig. 7b), semicircular regions as for the SiNWs's EIS; however, an approximately straight line with a slope of 45° was observed in the low-frequency region indicating a Warburg region, which is attributed to the diffusion transfer limitation of charged ions in the presence of aggregated Ni nanoparticles. Table 2 reports a significant decrease for the electron transfer resistance, which is due to the semiconductive properties of the nickel nanoparticles that make the electron transfer easier.

The Ni@SiNWs electrode possesses advantages that include extended time stability. It was investigated in a 0.1 M PBS solution containing 2.5 mM ferri-ferrocyanide as reported in Fig. 7c. These results demonstrate the excellent stability of prepared electrodes.

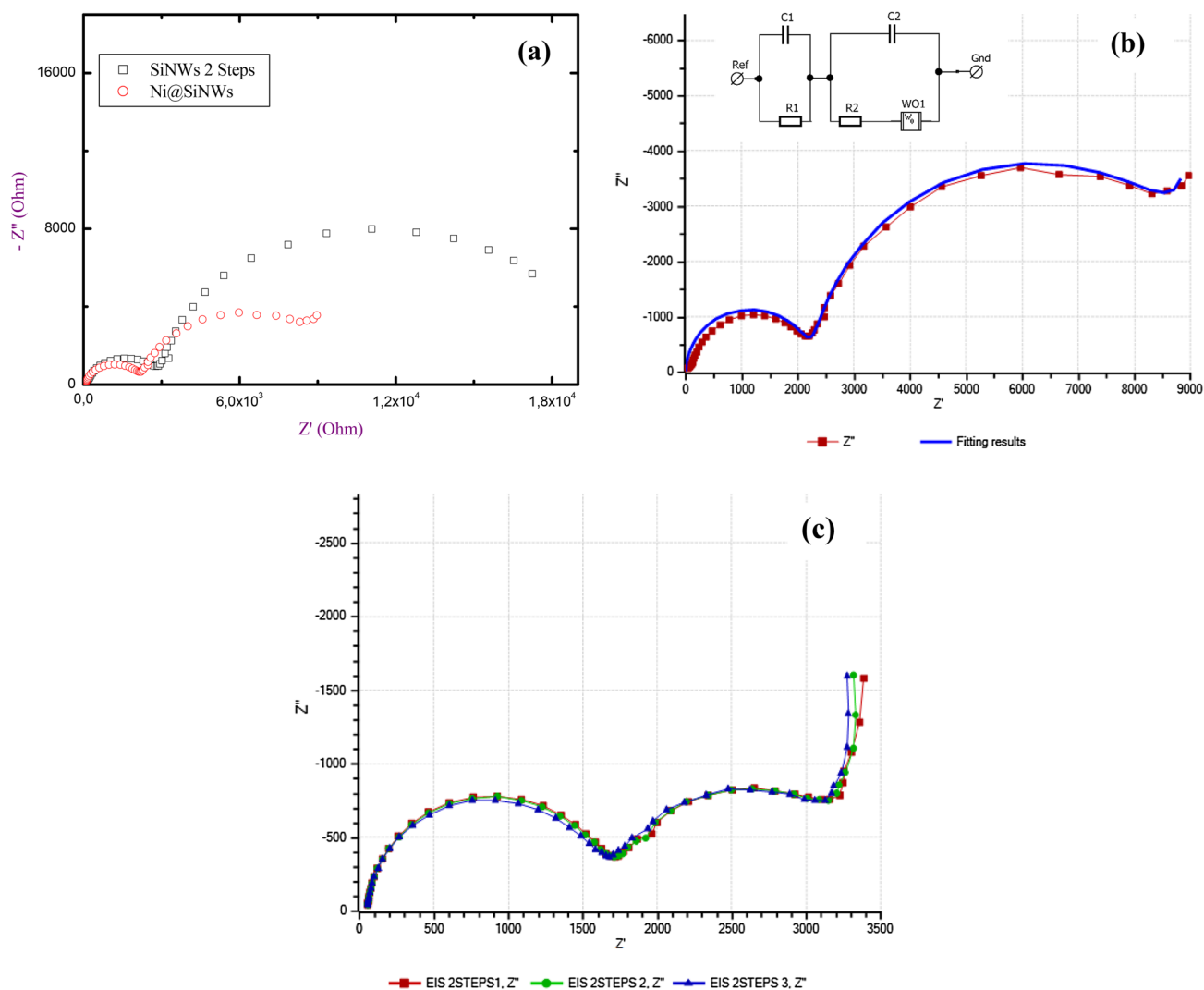


Fig. 7 a EIS Nyquist plots of SiNWs two-step technique and Ni@SiNWs template, b Fitting curve of EIS result of modified silicon nanowires and c Successive EIS scan of Ni@SiNWs in 2.5 mM ferri-ferrocyanide, 0.1 M PBS electrolyte proving the stability of the template

Table 2 The parameters of the equivalent circuit of Nyquist Plots of SiNWs two-step etching and Ni@SiNWs template

	R_1 (Ohm)	R_2 (Ohm)	C_1 (μ F)	C_2 (μ F)	W
Ni@SiNWs	6402.5	2156.0	4.63	0.06	1465.6

4 Conclusion

This work confirms that MACE technique in both methods (one-step and two-step) present successful and well-oriented silicon nanowires at room temperature. MACE technique presents several advantages including its simplicity and its low cost allowing the production of the nanostructure of silicon at room temperature without complex equipment.

The results indicate that the morphology of SiNWs strongly depends on the etchant used. In our work, the one-step and two-step MACE techniques affect the nucleation and mobility of Ag particles, which lead to a different length and density structure within the nanowires. Thus, the electrochemical properties of the surface are influenced. Therefore, in our study, we compared principally the resistance of the surface as well its capacitance using the cyclic voltammetry and the impedance measurements. We can observe a better result from the point of view of biosensing application for two-step MACE SiNWs, and as for the one-step MACE SiNWs, it shows a good responses for solar cells templates.

Acknowledgements This work was partly supported by the Nova Scotia Health Research(NSHRF) Establishment Grant for “Magnetic Nanoparticle Platform for Development of Wound Healing Sensor”

Project, the NSERC Discovery Grant for “Tunable Nanocomposites for Smart Materials and Technology Platform”, MITACS Career Connect, Clean Foundation, and CFI. Author FZ appreciate the technical assistance of Ms. Judy MacInnis of Chemistry Department of Cape Breton University, especially with TEM analysis. The authors appreciate also the participation of Dr. Muhammad Saqib of Fraunhofer-Institut für Keramische Technologien und Systeme IKTS for MEB analysis.

Declarations

Conflict of interest The authors declare that they have no known competing financial interests or personal relationships that could have appeared to influence the work reported in this paper.

References

- Rahmani M et al (2021) Effect of etching duration on the morphological and opto-electrical properties of silicon nanowires obtained by Ag-assisted chemical etching. *Silicon* 13(1):179–187. <https://doi.org/10.1007/s12633-020-00416-2>
- Naama S, Hadjersi T, Larabi A, Nezzal G (2021) Effect of silicon wafer resistivity on morphology and wettability of silicon nanowires arrays. *Silicon* 13:893–899. <https://doi.org/10.1007/s12633-020-00511-4>
- Lu W, Lieber CM (2006) Semiconductor nanowires. *J Phys D Appl Phys* 39(21):R387. <https://doi.org/10.1088/0022-3727/39/21/R01>
- Huang S, Zhang B, Shao Z, He L, Zhang Q, Jie J, Zhang X (2020) Ultraminiaturized stretchable strain sensors based on single silicon nanowires for imperceptible electronic skins. *Nano Lett* 20(4):2478–2485. <https://doi.org/10.1021/acs.nanolett.9b05217>
- Nuzaihan M, Hashim U, Arshad MM, Ruslinda AR, Rahman SFA, Fathil MFM, Ismail MH (2016) Top-down nanofabrication and characterization of 20 nm silicon nanowires for biosensing applications. *PloS ONE* 11(3):e0152318. <https://doi.org/10.1371/journal.pone.0152318>
- Jeribi M, Nafie N, Boujmil MF, Bouaicha M (2021) Response modulation of silicon nanowires-based sensor to carbon number in petroleum vapor detection. *Fuel* 304:121260. <https://doi.org/10.1016/j.fuel.2021.121260>
- Gautam V, Kumar A, Kumar R, Jain VK, Nagpal S (2021) Silicon nanowires/reduced graphene oxide nanocomposite based novel sensor platform for detection of cyclohexane and formaldehyde. *Mater Sci Semicond Process* 123:105571. <https://doi.org/10.1016/j.mssp.2020.105571>
- Wang Y, Wang T, Da P, Xu M, Wu H, Zheng G (2013) Silicon nanowires for biosensing, energy storage, and conversion. *Adv Mater* 25(37):5177–5195. <https://doi.org/10.1002/adma.201301943>
- Peng KQ, Lee ST (2011) Silicon nanowires for photovoltaic solar energy conversion. *Adv Mater* 23(2):198–215. <https://doi.org/10.1002/adma.201002410>
- Boukai AI, Bunimovich Y, Tahir-Kheli J, Yu JK, Goddard Iii WA, Heath JR (2008) Silicon nanowires as efficient thermoelectric materials. *Nature* 451(7175):168171. <https://doi.org/10.1038/nature06458>
- Elyamny S, Dimaggio E, Magagna S, Narducci D, Pennelli G (2020) High power thermoelectric generator based on vertical silicon nanowires. *Nano Lett* 20(7):4748–4753. <https://doi.org/10.1021/acs.nanolett.0c00227>
- Chan CK, Peng H, Liu G, McIlwrath K, Zhang XF, Huggins RA, Cui Y (2008) High-performance lithium battery anodes using silicon nanowires. *Nature Nanotechnol* 3(1):31. <https://doi.org/10.1038/nnano.2007.411>
- Tao B, He J, Miao F (2020) A hybrid sandwich structure of TiO₂/N-graphene/Ag supported by ordered silicon nanowires and its application as lithium-ion battery electrodes. *Mater Lett* 262:127046. <https://doi.org/10.1016/j.matlet.2019.127046>
- Fu YQ, Colli A, Fasoli A, Luo JK, Flewitt AJ, Ferrari AC, Milne WI (2009) Deep reactive ion etching as a tool for nanostructure fabrication. *J Vac Sci Technol B* 27(3):1520–1526. <https://doi.org/10.1116/1.3065991>
- Juhász R, Elfström N, Linnros J (2005) Controlled fabrication of silicon nanowires by electron beam lithography and electrochemical size reduction. *Nano Lett* 5(2):275280. <https://doi.org/10.1021/nl0481573>
- Sunkara MK, Sharma S, Miranda R, Lian G, Dickey EC (2001) Bulksynthesis of silicon nanowires using a low-temperature vapour-liquid-solid method. *Appl Phys Lett* 79(10):1546–1548. <https://doi.org/10.1063/1.1401089>
- Zaïbi F, Slama I, Okolie C, Deshmukh J, Hawco L, Mastouri M, Bennett C, Mkandawire M, Chtourou R (2020) Electro-performance of functionalized silicon nanowires by conductive polymer-coated with gold nanoparticles. *Colloids Surf A* 589:124450. <https://doi.org/10.1016/j.colsurfa.2020.124450>
- Singh N, Sahoo MK, Kale PG (2018) Effect of MACE parameters on length of porous silicon nanowires (PSiNWs). *J Cryst Growth* 496:10–14. <https://doi.org/10.1016/j.jcrysgro.2018.05.019>
- Leonardi AA, Faro MJL, Irrera A (2021) Silicon nanowires synthesis by metal-assisted chemical etching: a review. *Nanomaterials* 11(2):383. <https://doi.org/10.3390/nano11020383>
- Lam NTN, Giang NT, Kien PT, Dung ND, Ha NN (2019) N-type silicon nanowires prepared by silver metal-assisted chemical etching: fabrication and optical properties. *Mater Sci Semiconduct Process* 90:198–204. <https://doi.org/10.1016/j.mssp.2018.10.026>
- Nassiopoulou AG, Gianneta V, Katsogridakis C (2011) Si nanowires by a single step metal-assisted chemical etching process on lithographically defined areas: formation kinetics. *Nanoscale Res Lett* 6(1):597. <https://doi.org/10.1186/1556-276X-6-597>
- Osminkina LA, Gonchar KA, Marshov VS, Bunkov KV, Petrov DV, Golovan LA, Talkenberg F, Sivakov VA, Timoshenko VY (2012) Optical properties of silicon nanowire arrays formed by metal-assisted chemical etching: evidences for light localization effect. *Nanoscale Res Lett* 7(1):524. <https://doi.org/10.1186/1556-276X-7-524>
- Akan R, Parfeniukas K, Vogt C, Toprak MS, Vogt U (2018) Reaction control of metal-assisted chemical etching for silicon-based zone plate nanostructures. *RSC Adv* 8(23):12628–12634. <https://doi.org/10.1039/C8RA01627E>
- Gaidi M et al (2021) Enhanced photocatalytic activities of silicon nanowires/graphene oxide nanocomposite: effect of etching parameters. *J Environ Sci* 101:123–134. <https://doi.org/10.1016/j.jes.2020.08.010>
- Rahmani M, Amdouni S, Zaïbi MA, Meftah A (2020) Effect of etching duration on the morphological and opto-electrical properties of silicon nanowires obtained by Ag-assisted chemical etching. *Silicon*. <https://doi.org/10.1007/s12633-020-00416-2>
- Wendisch FJ, Abazari M, Mahdavi H, Rey M, Vogel N, Musso M, Diwald O, Bourret GR (2020) Morphology-graded silicon nanowire arrays via chemical etching: engineering optical properties at the nanoscale and macroscale. *ACS Appl Mater Interfaces* 12(11):13140–13147. <https://doi.org/10.1021/acsami.9b21466>
- Naffeti M, Postigo PA, Chtourou R, Zaïbi MA (2020) Elucidating the effect of etching time key-parameter toward optically and electrically-active silicon nanowires. *Nanomaterials* 10(3):404. <https://doi.org/10.3390/nano10030404>
- Ahmed N, Ramasamy P, Bhargav PB, Rayerfrancis A, Chandra B (2020) Development of silicon nanowires with optimized

- characteristics and fabrication of radial junction solar cells with < 100 nm amorphous silicon absorber layer. *Mater Sci Semiconduct Process* 106:104778. <https://doi.org/10.1016/j.mssp.2019.104778>
29. Ahoulou S, Perret E, Nedelec JM (2021) Functionalization and characterization of silicon nanowires for sensing applications: a review. *Nanomaterials* 11(4):999. <https://doi.org/10.3390/nano11040999>
30. Anwar AW, Majeed A, Iqbal N, Ullah W, Shuaib A, Ilyas U, Bibi F, Rafique HM (2015) Specific capacitance and cyclic stability of graphene based metal/metal oxide nanocomposites: a review. *J Mater Sci Technol* 31(7):699–707. <https://doi.org/10.1016/j.jmst.2014.12.012>
31. Tao B, Zhang J, Miao F, Hui S, Wan L (2010) Preparation and electrochemistry of NiO/SiNW nanocomposite electrodes for electrochemical capacitors. *Electrochim Acta* 55(18):5258–5262. <https://doi.org/10.1016/j.electacta.2010.04.057>

Publisher's Note Springer Nature remains neutral with regard to jurisdictional claims in published maps and institutional affiliations.